Ironing the Modulo Folds: Unlimited Sensing with 100x Bandwidth Expansion

Yuliang Zhu, Ruiming Guo and Ayush Bhandari
Dept. of Electrical and Electronic Engg., Imperial College London, SW7 2AZ, UK.
{yuliang.zhu19,ruiming.guo,a.bhandari}@imperial.ac.uk

***Abstract*—The practical implementation of Shannon's sampling theorem using analog-to-digital converters (ADCs) involves an inescapable trade-off between dynamic range and digital resolution. The Unlimited Sensing Framework (USF) overcomes this fundamental limitation by leveraging a co-design of modulo folding in hardware with algorithmic unfolding (or ironing) in software. While recent years have seen progress on both hardware and algorithmic fronts, further technological advancements are needed to push the bandwidth (BW) limits of modulo ADC hardware. Can higher bandwidths be achieved through algorithms alone? In this paper, we take a computational sensing approach to enhance the operational capabilities of modulo ADCs by shifting the emphasis from precise, resource-intensive hardware to algorithmic solutions. As a result, we demonstrate a 100-fold bandwidth expansion beyond the modulo ADC's technical specifications. Our key contributions include: the mathematical formalization of the bandwidth expansion problem based on phenomenological observations of high-frequency non-linear effects, a sampling theorem that provides recovery guarantees for our algorithm, and hardware validation demonstrating the practical advantages of our method.**

***Index Terms*—Analog-to-digital converters (ADCs), bandwidth, sampling theory, super-resolution, unlimited sensing.**

I. Introduction

The Unlimited Sensing Framework (USF) [1]–[4] is built on a simple yet powerful mathematical insight: *for smooth functions, their fractional part encodes the integer part*. This insight leads to a novel digital sensing pipeline that redefines digital acquisition, representation, and processing.

Why is this significant? Conventional ADCs work on the Shannon-Nyquist principle and quantize the input signal (integer part) with the resulting quantization noise (fractional part) imposing a fundamental limit on digital resolution. One aspect which is less considered in mathematical sampling and approximation theory is the *saturation problem*—when the dynamic range of the input signal exceeds the ADC's capacity, it can lead to saturation [5], [6] or clipping loss [7], [8], rendering the sampled signal nearly useless. In contrast, USF demonstrates that signals can be reconstructed from quantization noise (fractional part) [9], overcoming the saturation problem and achieving high digital resolution within a given bit budget.

This work is supported by the European Research Council's Starting Grant for "CoSI-Fold" (101166158) and UK Research and Innovation council's FLF Program "Sensing Beyond Barriers via Non-Linearities" (MRC Fellowship award no. MR/Y003926/1). Further details on Unlimited Sensing and materials on *reproducible research* are available via `https://bit.ly/USF-Link`.

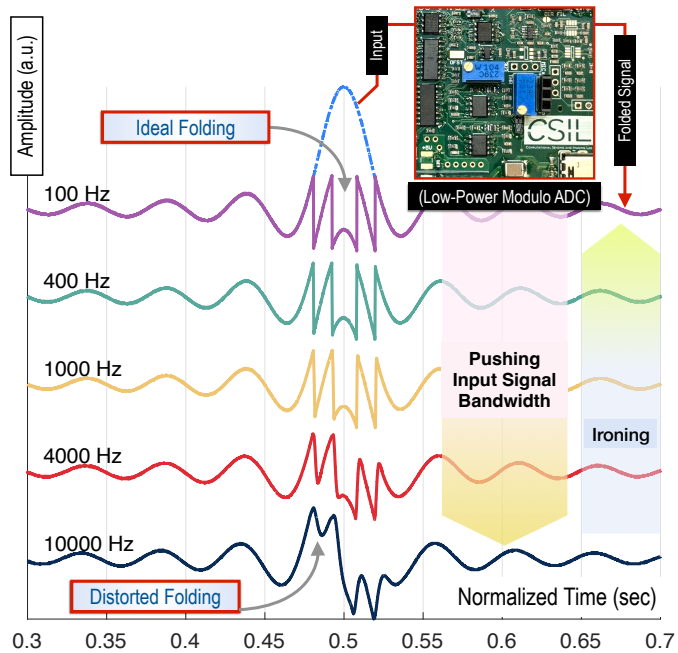

Fig. 1: Folding of the bandlimited Dirichlet kernel using USF hardware [3], [4], [10], [11] generates the fractional part, or the continuous-time modulo signal. We demonstrate the impact of pushing the bandwidth beyond the low-power hardware's design limit, originally intended for an input bandwidth of 1 kHz. For reconstruction from these measurements, see Fig. 4, and also Fig. 5.

As shown in Fig. 1, in the USF, the quantization noise is acquired in the analog domain, prior to sampling, by implementing modulo non-linearity in hardware [3], [4], [11]

$$\mathscr{M}_\lambda : g \mapsto 2\lambda\left(\left[\!\left[\frac{g}{2\lambda}+\frac{1}{2}\right]\!\right]-\frac{1}{2}\right), \quad \begin{array}{l}[\![g]\!] \stackrel{\text{def}}{=} g-\lfloor g\rfloor \\ \lambda>0\end{array} \tag{1}$$

where $\lfloor\cdot\rfloor$ denotes the integer part of g. Akin to the Shannon-Nyquist sampling theorem, despite modulo folding, the sampling theorem in USF [1], [2] proves that sampling or time quantization is lossless. The remaining loss comes from amplitude quantization, for which it is well known that the ADCs expend their power linearly with oversampling but exponentially with bit-budget [12]. Hence, the USF is power efficient because for the same bit budget, it quantizes a much smaller dynamic range offering *digital super-resolution* in addition to eliminating the saturation problem. Hardware validation of the USF has shown a 60-fold dynamic range extension in practice [11] together with a 10 dB improvement in the quantization noise floor in applications *e.g.* radar [13] and tomography [14].

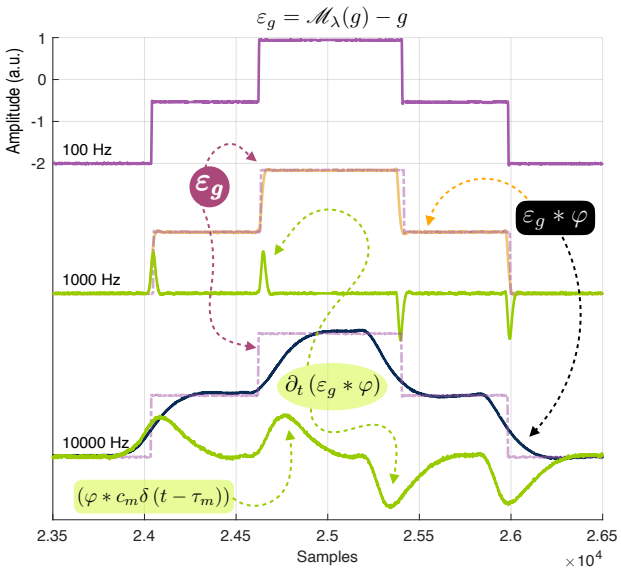

Fig. 2: Hardware calibration of the residue $\varepsilon_g = g - \mathscr{M}_\lambda(g)$ (see (1)) via controlled experiment, with optimal input BW *e.g.* 100 Hz. The evolution of non-linearity is shown as it becomes more pronounced with increasing input BW at 1000 Hz and 10000 Hz, corresponding to the measurements in Fig. 1. Extensive experiments reveal that the behavior of the residue at higher BWs is related to the ideal BW residue through low-pass projections with a φ.

Phenomenological Observations. Since the development of our first hardware in [3], we have been actively developing the USF hardware [10], [11], [13], [15], which has continuously guided our theoretical and algorithmic progress. Experimental observations (see Fig. 1) reveal that when the folding hardware is pushed beyond its designed BW specifications, the folded signal experiences a new form of distortion. Although modulo hardware has been developed in subsequent works [16], such observations have not been reported in previous studies.

As shown in Fig. 2, sweeping through higher input BWs reveals non-linearity in the residue, defined as $\varepsilon_g = g - \mathscr{M}_\lambda(g)$. Our key observation is that residues at higher input BWs are related to the residue under ideal BW conditions through a low-pass projection. This experimental insight motivates the development of a new algorithm that directly addresses hardware non-idealities in the digital domain. Current algorithms are not designed to handle such cases, partly due to the novelty of this observation and the existing divide between theory and hardware. An algorithm for *Bandwidth Expansion* [17], [18], *i.e.* recovering the input in the presence of high BW non-linearities is highly desirable, as it enables the **efficient use of low-cost hardware beyond its prescribed specifications**.

Contributions. Embodying the spirit of *computational sensing*, our contributions lie at the intersection of theory, algorithms, hardware, and experiments. Specifically, we: i) Formalize the bandwidth expansion problem by identifying the underlying mathematical forward model. ii) Develop an efficient algorithm with noise resilience and super-resolution capabilities, supported by a recovery guarantee. iii) Demonstrate a 100-fold bandwidth expansion through hardware experiments, highlighting the effectiveness of the proposed approach.

II. From Observations to a Mathematical Model

Let $g \in \mathcal{B}_{\Omega_g}$ be a bandlimited input. The ideal modulo-folded samples are given by $y[n] = \mathscr{M}_\lambda(g(t))|_{t=nT}$, where $T > 0$ is the sampling period. When pushing the BW of the modulo ADC hardware or $\mathscr{M}_\lambda$–ADC, the folding rate is constrained by the response of the slowest switching component (*e.g.* slew rate [19]). Through extensive experiments, we have observed that the non-ideal deviation from (1) can be modeled as $\mathscr{Q}(\mathscr{M}_\lambda(g))$, where $\mathscr{Q}(\cdot)$ represents an unknown non-linearity. Interestingly, our experiments reveal that the following approximation holds across a wide range of BWs:

$$\mathscr{Q}(\mathscr{M}_\lambda(g))(t) \approx (\varphi * \mathscr{M}_\lambda(g))(t) \stackrel{\text{def}}{=} y_{\Omega_g}(t). \tag{2}$$

This model suggests that the unknown non-linearity $\mathscr{Q}(\cdot)$ is empirically equivalent to a low-pass projection of $\mathscr{M}_\lambda(\cdot)$, where $\varphi(\cdot)$ accounts for accumulated inertia—previously observed in a different form as *hysteresis* [20]. The setup is backwards compatible with the ideal modulo non-linearity because, under optimal BW conditions, $\mathscr{Q} \to$ Identity $\Rightarrow \varphi \to \delta$.

Existing recovery algorithms [2], [3], [21]–[25] are not designed to handle such non-idealities unless $\mathscr{Q}$ is the identity operator, and thus fail to recover g in the presence of distortions. The goal of this paper is to develop a robust recovery method for reconstructing the bandlimited input signal g from the distorted folded samples $\{y_{\Omega_g}[n]\}_{n\in\mathbb{I}_N}$, thereby computationally extending the effective BW of $\mathscr{M}_\lambda$–ADC.

III. Signal Recovery via Algorithmic Bandwidth Expansion

In this section, our goal is to map the recovery problem into an "Additive Super-Resolution" problem. The starting point is the modular decomposition property [1], leading to

$$g = \mathscr{M}_\lambda(g) + \varepsilon_g, \quad \varepsilon_g(t) = \sum_{m=0}^{M-1} c_m \mathbb{1}(t - \tau_m). \tag{3}$$

where $c_m \in 2\lambda\mathbb{Z}$ and $\tau_m \in T\mathbb{Z}^+$ represent the fold amplitude and instant, respectively. In view of (2), we can write,

$$y_{\Omega_g} = \varphi * \mathscr{M}_\lambda(g) \equiv g * \varphi - \varepsilon_g * \varphi, \qquad \varphi \in \mathcal{B}_{\Omega_\varphi} \tag{4}$$

and given that ε_g is a simple function [2], its total-variation results in a sparse representation. Consequently, we note that,

$$\begin{aligned} \partial_t y_\Omega &= \overbrace{\partial_t(g * \varphi)}^{\in \mathcal{B}_{\Omega_g}} - \overbrace{\partial_t(\varepsilon_g * \varphi)}^{\text{(see Fig. 2)}} \\ &= \underbrace{\partial_t(g * \varphi) - \sum_{m=0}^{M-1} c_m \varphi(\cdot - \tau_m)}_{\text{Additive Super-Resolution}} \end{aligned} \tag{5}$$

which is an *additive super-resolution* problem where the recovery entails separation of the additive terms: i) $\partial g \in \mathcal{B}_{\Omega_g}$ and, ii) low-pass projections of spikes. The sampled version of the problem can be formulated as the recovery of g from,

$$y_{\Omega_g}[n] \stackrel{(4)}{=} (\varphi * y)[n] = (\varphi \circledast \mathscr{M}_\lambda(g))[n], \quad n \in \mathbb{I}_N. \tag{6}$$

where $\circledast$ denotes circular convolution and $\mathbb{I}_N = \{0, \ldots N-1\}$.

Theorem 1. *Let $g \in \mathcal{B}_{\Omega_g}$ and $\varphi \in \mathcal{B}_{\Omega_\varphi}$. Suppose we are given measurements, $y_{\Omega_g}[n]$ in (6) and φ is known.*

Then, $\{g[n]\}_{n\in\mathbb{I}_N}$ can be perfectly recovered (up to a constant), provided that $N_\varphi - N_g \geqslant 2M$, where $N_g \stackrel{\text{def}}{=} \lceil \Omega_g T(N-1)/(2\pi)\rceil$ and M is the number of folds.

Proof. In view of (6) and (3), we have $y_{\Omega_g}[n] = \varphi[n] \circledast g[n] - \varphi[n] \circledast \varepsilon_g[n]$. Let $\underline{g}[n] = g[n+1] - g[n]$ denote the finite difference. Then,

$$\underline{y}_{\Omega_g}[n] = \varphi[n] \circledast \underline{g}[n] - \varphi[n] \circledast \underline{\varepsilon}_g[n], \quad n \in \mathbb{I}_{N-1}. \tag{7}$$

In above, $\underline{y}_{\Omega_g}$ can be decomposed into, a) bandlimited term: $\varphi \circledast \underline{g}$ with BW $\min(\Omega_g, \Omega_\varphi)$ (In practice, $\Omega_\varphi > \Omega_g$), and b) low-pass projections of spikes, $(\varphi \circledast \underline{\varepsilon}_g)$, since $\underline{\varepsilon}_g[n] = \sum_{m=0}^{M-1} c_m \delta[n - \tau_m/T]$, (see Fig. 2), where $\delta[\cdot]$ denotes the Kronecker delta.

Fourier-Domain Separation. From the sampled representation in (7), we observe a separability [3] in the Fourier domain that leads to model simplification. Let $\widehat{\underline{g}}$ denote the DFT (Discrete Fourier Transform) of $\underline{g}$, then, (7) maps to,

$$\widehat{\underline{y}}_{\Omega_g}[k] = \widehat{\varphi}[k]\,\widehat{\underline{g}}[k] - \widehat{\varphi}[k]\,\widehat{\underline{\varepsilon}}_g[k], \quad k \in \mathbb{I}_{N-1} \tag{8}$$

where $\widehat{\underline{\varepsilon}}_g$ is a sum of complex exponentials given by,

$$\widehat{\underline{\varepsilon}}_g[k] = \sum\nolimits_{m=0}^{M-1} c_m e^{\frac{-\jmath 2k\pi\tau_m}{(N-1)T}} \tag{9}$$

which spans the entire digital frequency band. However, note

$$(\widehat{\varphi}\widehat{\underline{g}})[k] = 0, \quad k \in [0, N_g] \cup [N-2-N_g, N-2] \tag{10}$$

where $N_g \stackrel{\text{def}}{=} \lceil \Omega_g T(N-1)/(2\pi)\rceil$. Consequently, we obtain

$$\widehat{\underline{y}}_{\Omega_g}[k] \stackrel{(8)}{=} -\widehat{\varphi}[k]\,\widehat{\underline{\varepsilon}}_g[k], \quad k \in [N_g+1, N-3-N_g]. \tag{11}$$

Note that $\widehat{\varphi}[k] = 0$ if $k \in [0, N_\varphi] \cup [N-2-N_\varphi, N-2]$, where $N_\varphi \stackrel{\text{def}}{=} \lceil \Omega_\varphi T(N-1)/(2\pi)\rceil$. Hence, $\widehat{\underline{\varepsilon}}_g$ can be found

$$\widehat{\underline{\varepsilon}}_g[k] \stackrel{(11)}{=} -\widehat{\underline{y}}_{\Omega_g}[k]/\widehat{\varphi}[k], \quad k \in [N_g+1, N_\varphi]. \tag{12}$$

Residue Recovery via Prony's Method. Having known $\widehat{\underline{\varepsilon}}_g[k]$, $-\widehat{\underline{y}}_{\Omega_g}[k]/\widehat{\varphi}[k] = \widehat{\underline{\varepsilon}}_g[k] \equiv \sum_{m=0}^{M-1} c_m e^{-\jmath\frac{2k\pi\tau_m}{T(N-1)}}$ where $\tau_m/T \in \mathbb{I}_{N-1}$, the fold parameters $\{c_m, \tau_m\}_{m\in\mathbb{I}_M}$ can be found using the Prony's method [26]: let $f[k]$ with $k \in \mathbb{I}_{M+1}$ be the filter with z-transform $\widehat{f}(z) = \sum_{k=0}^{M} f[k] z^{-k} = \prod_{m=0}^{M-1}(1 - u_m z^{-1})$ where $u_m = e^{-\jmath 2\pi\tau_m/(T(N-1))}$. The roots of $\widehat{f}(z)$ uniquely determines the folding locations of interest. Then, it follows that f annihilates the complex exponential sequence $\widehat{\underline{\varepsilon}}_g[k], k \in [N_g+1, N_\varphi]$:

$$\begin{aligned}\left(\widehat{\underline{\varepsilon}}_g * f\right)[k] &= \sum\nolimits_{l=0}^{M} f[l]\,\widehat{\underline{\varepsilon}}_g[k-l] \\ &= \sum\nolimits_{l=0}^{M} f[l] \sum\nolimits_{m=0}^{M-1} c_m e^{-\jmath\frac{2(k-l)\pi\tau_m}{T(N-1)}} \\ &= \sum\nolimits_{m=0}^{M-1} c_m e^{-\jmath\frac{2k\pi\tau_m}{T(N-1)}} \sum\nolimits_{l=0}^{M} f[l]\, u_m^{-l} = 0.\end{aligned} \tag{13}$$

In vector-matrix form, (13) can be written as $\mathbf{A}\mathbf{f} = \mathbf{0}$ where $\mathbf{A}$ is the Toeplitz matrix constructed by $\widehat{\underline{\varepsilon}}_g$. Given $\mathbf{A}$ is rank deficient, we can find the filter coefficients $\{f[k]\}_{k\in\mathbb{I}_M}$ by solving the above system of equations, provided that $N_\varphi - N_g \geqslant 2M$. Thereafter, $\{\tau_m\}_{m\in\mathbb{I}_M}$ can be estimated by computing the roots of $\widehat{f}(z)$ and amplitudes $\{c_m\}_{m\in\mathbb{I}_M}$ are found via least-squares. Given $\{c_m, \tau_m\}$, the residue is reconstructed using (3), leading to $y_{\Omega_g} + \varepsilon_g * \varphi \to \varphi * g$. Given $g \in \mathcal{B}_{\Omega_g}$ and $\Omega_\varphi > \Omega_g$, g can be reconstructed via inverse filtering

$$g = \mathsf{IDFT}\left(\mathbb{1}_{[-\Omega_g,\Omega_g]}\widehat{g}_\varphi/\widehat{\varphi}\right), \quad g_\varphi = y_{\Omega_g} + \varepsilon_g * \varphi \tag{14}$$

where $\mathbb{1}_{[\cdot]}$ is the indicator function, $\widehat{g}_\varphi$ is the DFT of g_φ and IDFT denotes the inverse Discrete Fourier Transform. □

Algorithm 1 Bandwidth Expansion in USF

Input: Folded measurements $\{y_{\Omega_g}[n]\}_{n\in\mathbb{I}_N}$ and φ.

1: Compute the DFT of $\underline{y}_{\Omega_g}$.
2: Evaluate $\widehat{\underline{\varepsilon}}_g[k], k \in [N_g+1, N_\varphi]$ via (9).
3: Find $\{f[k]\}_{k\in\mathbb{I}_{M+1}}$ via (13).
4: Estimate $\{c_m, \tau_m\}_{m\in\mathbb{I}_M}$.
5: Recover ε_g using (3).
6: Reconstruct g using (14).

Output: The recovered bandlimited signal g.

Algorithmic Implementation. Theorem 1 leads to an efficient algorithm outlined in Algorithm 1 and validated in Section IV. For estimating $\{c_m, \tau_m\}$, we employ the *Matrix Pencil Method* [27], which provides improvements over Prony's method[1]. The number of folds (M) can be determined using methods like *second-order statistic of eigenvalues* (SORTE) [31].

IV. Experiments

The overarching goal of the this section is to demonstrate bandwidth expansion of $\mathscr{M}_\lambda$–ADC is feasible in practice. By intentionally increasing the input signal BW way beyond the technical specifications of the $\mathscr{M}_\lambda$–ADC, we introduce measurement distortions at the hardware level and recover the original input using advanced algorithms. This is made possible by *ironing the modulo folds* that get distorted during the BW expansion. Through our numerical simulations and hardware experiments, we demonstrate precise signal recovery, made possible by the co-design of hardware and algorithms.

A. Numerical Tests on Noise Resilience.

We first conduct the following numerical tests to evaluate the robustness of the proposed algorithm in the presence of noise. The input g has a BW of 1 kHz with $\|g\|_\infty = 1$. We set $\lambda = 0.10$ and generate ideal, noiseless folded samples as $y[n] = \mathscr{M}_\lambda(g(nT)), n \in \mathbb{I}_N$, where $T = 4.0$ μs, $M = 20$, and $N = 24990$. The noisy, distorted samples are yielded as $y_{\Omega_g,w}[n] = (\varphi * \mathscr{M}_\lambda(g))(nT) + w[n]$, $w \backsim \mathcal{N}(0, \sigma^2)$ where φ is obtained from hardware experiments to mimic real-world conditions. For each noise level σ, the recovery error is computed by averaging results over 1000 random noise realizations. The performance of the proposed algorithm

[1]Other high-resolution spectral estimation techniques, such as those proposed in [28]–[30], are also applicable.

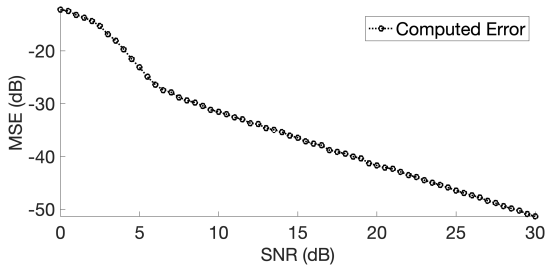

Fig. 3: Recovery MSE vs SNR. The result at each SNR sample is averaged over 1000 random realizations. The dynamic range is $\|g\|_\infty = 10\lambda$. Our method offers accurate recovery up to a low SNR (5 dB).

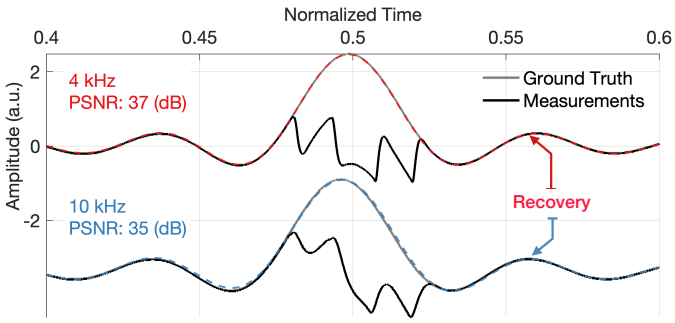

Fig. 4: Fold Separation with Super-Resolution. The localized nature of the input Dirichlet kernels results in closely spaced folds near the peak ($M = 4$). From top to bottom, the BW is progressively increased (from 4 to 10 kHz, corresponding to the data in Fig. 1), leading to increasingly pronounced folding non-idealities. Despite the challenges associated with fold separation, accurate recovery is achieved across all scenarios.

across SNR levels ranging from 0 to 30 dB is shown in Fig. 3. As demonstrated in Fig. 3, the proposed algorithm achieves accurate reconstruction down to SNR = 5 dB, showcasing its superior resilience to noise effects.

B. Hardware Experiments.

Protocol. In the first experiment, we use *localized, bandlimited Dirichlet kernels*, shown in Fig. 1 to assess the ability to separate closely spaced folds—a critical capability when dealing with high dynamic range inputs. In the second experiment, we push the input signal BW to 10^5 Hz, exceeding the $\mathscr{M}_\lambda$–ADC 's design limit of handling up to 10^3 Hz. The φ is obtained through experimental calibration and remains fixed throughout the experiments. For each setup, the distorted folded samples are captured directly from the $\mathscr{M}_\lambda$–ADC. Simultaneously, the input and output of the $\mathscr{M}_\lambda$–ADC are recorded using the PicoScope 3406D oscilloscope, providing ground truth and measurement data, respectively. In each experiment, we fix the signal waveform and the system response φ, progressively increasing the BW: from $4 \rightarrow 10$ kHz in Fig. 4 and from $20 \rightarrow 100$ kHz in Fig. 5.

Experiment 1: Super-Resolved Folds. The input signal BW ranges from 4 to 10 kHz, with $\|g\|_\infty = 2.52$. We set $\lambda = 0.77$ and $T = 16.0$ μs, resulting in $M = 4$ folds and $N = \{12508, 5001\}$ for $\{4, 10\}$ kHz, respectively. At higher input BWs, resolving two adjacent folds becomes challenging as their separation approaches the time span of the system response φ. This difficulty is particularly noticeable at 10 kHz, as shown in Fig. 4. Despite these challenges, the proposed algorithm successfully reconstructs the signal, achieving a PSNR of over 35 dB. This highlights its high-resolution capability and effectiveness in handling closely spaced folds.

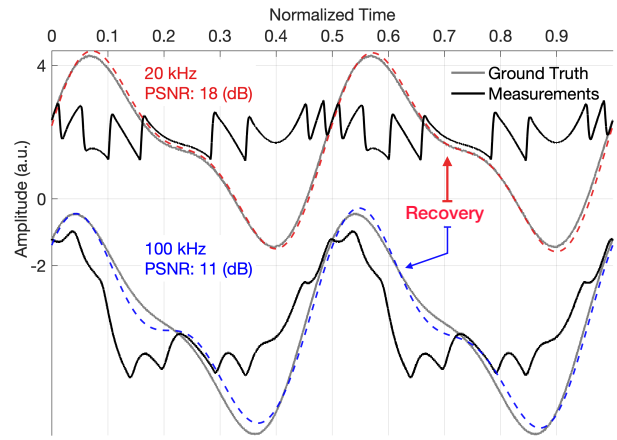

Fig. 5: 100x Bandwidth Expansion. To further evaluate the merits of the BW expansion method, the input BW is pushed from 20 kHz to 100 kHz, where the folding behavior becomes highly distorted and visually unrecognizable. In contrast, the proposed method demonstrates robust performance, achieving reasonabe reconstructions even at 100 kHz.

Experiment 2: Bandwidth Expansion. In the second experiment, $T = 4.0$ ns, $\|g\|_\infty = 4.32$ with $\lambda = 0.79$, resulting in $M = 16$ folds and $N = \{25002, 10004\}$ for $\{20, 100\}$ kHz, respectively. The BW of g is progressively increased from 2×10^4 to 10^5 Hz to evaluate the algorithm's performance under extreme conditions. As shown in Fig. 5, the measurements are severely distorted and difficult to interpret as the BW grows, presenting significant challenges for recovery. However, the proposed method demonstrates robust performance, achieving accurate reconstruction even at 10^5 Hz, thereby enabling a 100-fold BW expansion.

V. Conclusion

In recent years, the Unlimited Sensing Framework (USF) has emerged as a digital acquisition method capable of simultaneously achieving high dynamic range and digital resolution. This is enabled by modulo ADCs, which perform signal folding in analog hardware. Our experimental observations reveal that when the modulo ADC is pushed beyond its designed bandwidth specifications, the folded signal experiences a new form of distortion attributed to non-linearities. Our work shows that this distortion can be empirically modeled as an additive super-resolution problem, motivating the development of novel recovery methods. In this paper, we presented an efficient algorithm with super-resolution capabilities, backed by a recovery guarantee. Through hardware experiments, we demonstrated a 100-fold bandwidth expansion, highlighting the practical effectiveness of our approach. Our method facilitates the efficient use of low-cost USF hardware beyond its prescribed specifications, providing a pathway to extend the operational limits of USF enabled digital acquisition systems.

References

[1] A. Bhandari, F. Krahmer, and R. Raskar, "On unlimited sampling," in *Intl. Conf. on Sampling Theory and Applications (SampTA)*, Jul. 2017.

[2] ——, "On unlimited sampling and reconstruction," *IEEE Trans. Sig. Proc.*, vol. 69, pp. 3827–3839, Dec. 2020.

[3] A. Bhandari, F. Krahmer, and T. Poskitt, "Unlimited sampling from theory to practice: Fourier-Prony recovery and prototype ADC," *IEEE Trans. Sig. Proc.*, pp. 1131–1141, Sep. 2021.

[4] D. Florescu and A. Bhandari, "Time encoding via unlimited sampling: Theory, algorithms and hardware validation," *IEEE Trans. Sig. Proc.*, pp. 1–13, Sep. 2022.

[5] A. Nardecchia, V. Motto-Ros, and L. Duponchel, "Saturated signals in spectroscopic imaging: Why and how should we deal with this regularly observed phenomenon?" *Analytica Chimica Acta*, vol. 1157, no. 338389, pp. 1–9, May 2021.

[6] M. Hirsch, S. Harmeling, S. Sra, and B. Schölkopf, "Online multi-frame blind deconvolution with super-resolution and saturation correction," *Astronomy & Astrophysics*, vol. 531, p. A9, May 2011.

[7] J. Abel and J. Smith, "Restoring a clipped signal," in *IEEE Intl. Conf. on Acoustics, Speech, and Signal Processing*, Apr. 1991.

[8] F. Esqueda, S. Bilbao, and V. Valimaki, "Aliasing reduction in clipped signals," *IEEE Trans. Sig. Proc.*, vol. 64, no. 20, pp. 5255–5267, Oct. 2016.

[9] A. Bhandari and F. Krahmer, "HDR imaging from quantization noise," in *IEEE Intl. Conf. on Image Processing (ICIP)*, Oct. 2020, pp. 101–105.

[10] R. Guo, Y. Zhu, and A. Bhandari, "Sub-Nyquist USF spectral estimation: K frequencies with $6K + 4$ modulo samples," *IEEE Trans. Sig. Proc.*, vol. 72, pp. 5065–5076, 2024.

[11] Y. Zhu and A. Bhandari, "Unleashing dynamic range and resolution in unlimited sensing framework via novel hardware," in *2024 IEEE SENSORS*. IEEE, Oct. 2024, pp. 1–4.

[12] R. Walden, "Analog-to-digital converter survey and analysis," *IEEE J. Sel. Areas Commun.*, vol. 17, no. 4, pp. 539–550, Apr. 1999.

[13] T. Feuillen, B. S. M. R. Rao, and A. Bhandari, "Unlimited sampling radar: Life below the quantization noise," in *IEEE Intl. Conf. on Acoustics, Speech and Signal Processing (ICASSP)*, Jun. 2023.

[14] M. Beckmann, A. Bhandari, and M. Iske, "Fourier-domain inversion for the modulo Radon transform," *IEEE Trans. Comput. Imaging*, vol. 10, pp. 653–665, Apr. 2024.

[15] Y. Zhu, R. Guo, P. Zhang, and A. Bhandari, "Frequency estimation via sub-Nyquist unlimited sampling," in *IEEE Intl. Conf. on Acoustics, Speech and Signal Processing (ICASSP)*, Apr. 2024.

[16] S. Mulleti, E. Reznitskiy, S. Savariego, M. Namer, N. Glazer, and Y. C. Eldar, "A hardware prototype of wideband high-dynamic range analog-to-digital converter," *IET Circuits, Devices Systems*, vol. 17, no. 4, pp. 181–192, Jun. 2023.

[17] Z. Reznic, M. Feder, and R. Zamir, "Distortion bounds for broadcasting with bandwidth expansion," *IEEE Trans. Inf. Theory*, vol. 52, no. 8, pp. 3778–3788, Aug. 2006.

[18] K. Li and C.-H. Lee, "A deep neural network approach to speech bandwidth expansion," in *IEEE Intl. Con. on Acoustics, Speech and Signal Proc. (ICASSP)*. IEEE, Apr. 2015, pp. 4395–4399.

[19] Y. Geerts, M. Steyaert, and W. Sansen, "A high-performance multibit $\Delta\Sigma$ CMOS ADC," *IEEE J. Solid-State Circuits*, vol. 35, no. 12, pp. 1829–1840, Dec. 2000.

[20] D. Florescu, F. Krahmer, and A. Bhandari, "The surprising benefits of hysteresis in unlimited sampling: Theory, algorithms and experiments," *IEEE Trans. Sig. Proc.*, vol. 70, pp. 616–630, Jan. 2022.

[21] R. Guo and A. Bhandari, "ITER-SIS: Robust unlimited sampling via iterative signal sieving," in *IEEE Intl. Conf. on Acoustics, Speech and Signal Processing (ICASSP)*, Jun. 2023.

[22] ——, "Unlimited sampling of FRI signals independent of sampling rate," in *IEEE Intl. Conf. on Acoustics, Speech and Signal Processing (ICASSP)*, Jun. 2023.

[23] O. Ordentlich, G. Tabak, P. K. Hanumolu, A. C. Singer, and G. W. Wornell, "A modulo-based architecture for analog-to-digital conversion," *IEEE J. Sel. Topics Signal Process.*, vol. 12, no. 5, pp. 825–840, Oct. 2018.

[24] S. Rudresh, A. Adiga, B. A. Shenoy, and C. S. Seelamantula, "Wavelet-based reconstruction for unlimited sampling," in *IEEE Intl. Conf. on Acoustics, Speech and Signal Processing (ICASSP)*. IEEE, Apr. 2018, pp. 4584–4588.

[25] S. B. Shah, S. Mulleti, and Y. C. Eldar, "Lasso-based fast residual recovery for modulo sampling," in *IEEE Intl. Conf. on Acoustics, Speech and Sig. Proc. (ICASSP)*. IEEE, Jun. 2023.

[26] G. du Prony, "Essai experimental et analytique sur les lois de la dilatabilite de fluides elastiques et sur celles da la force expansion de la vapeur de l'alcool, a differentes temperatures," *Journal de l'Ecole Polytechnique*, vol. 1, no. 22, pp. 24–76, 1795.

[27] Y. Hua and T. Sarkar, "Matrix pencil method for estimating parameters of exponentially damped/undamped sinusoids in noise," *IEEE Trans. Acoust., Speech, Signal Process.*, vol. 38, no. 5, pp. 814–824, May 1990.

[28] B. N. Bhaskar, G. Tang, and B. Recht, "Atomic norm denoising with applications to line spectral estimation," *IEEE Trans. Sig. Proc.*, vol. 61, no. 23, pp. 5987–5999, Dec. 2013.

[29] R. Guo, Y. Li, T. Blu, and H. Zhao, "Vector-FRI recovery of multi-sensor measurements," *IEEE Trans. Sig. Proc.*, vol. 70, pp. 4369–4380, 2022.

[30] R. Guo and T. Blu, "Super-resolving a frequency band," *IEEE Signal Process. Mag.*, vol. 40, no. 7, pp. 73–77, Nov. 2023.

[31] Z. He, A. Cichocki, S. Xie, and K. Choi, "Detecting the number of clusters in n-way probabilistic clustering," *IEEE Trans. Pattern Anal. Mach. Intell.*, vol. 32, no. 11, pp. 2006–2021, Nov. 2010.